Phys. Status Solidi A **210,** No. 6, 1183–1189 (2013) / **DOI** 10.1002/pssa.201228589

physica status solidi a
www.pss-a.com
applications and materials science

Thermoelectric properties of Ce-doped n-type $Ce_xBi_{2-x}Te_{2.7}Se_{0.3}$ nanocomposites

Fang Wu[1,2], Hongzhang Song[1], Jianfeng Jia[1], Feng Gao[1], Yingjiu Zhang[1], and Xing Hu[*,1]

[1] School of Physical Engineering and Laboratory of Material Physics, Zhengzhou University, Zhengzhou 450052, P. R. China
[2] Department of Physics, Henan Institute of Education, Zhengzhou 450053, P. R. China

Received 2 September 2012, revised 31 January 2013, accepted 4 February 2013
Published online 25 February 2013

Keywords doping, hydrothermal synthesis, nanostructures, selenides, tellurides, thermoelectric properties

[*] Corresponding author: e-mail xhu@zzu.edu.cn, Phone: 86 37167767671, Fax: 86 37167766629

Ce-doped $Ce_xBi_{2-x}Te_{2.7}Se_{0.3}$ ($x = 0$–0.3) nanopowders were synthesized by the hydrothermal method and the obtained nanopowders were hot-pressed into bulk at 673 K under a pressure of 60 MPa in vacuum. The results show that Ce doping has significant effects on the morphologies of the nanopowders. With increasing Ce doping amount the morphology of the nanopowder changes from nanosheets to nanorods. The thermoelectric (TE) properties measurements show that Ce doping can increase the electrical conductivity greatly, but has little effect on improving Seebeck coefficient and thermal conductivity. There is an optimum value of Ce doping amount. The $Ce_{0.2}Bi_{1.8}Se_{0.3}Te_{2.7}$ sample shows a highest figure of merit of 0.85 at 413 K as compared to other samples prepared in same conditions.

© 2013 WILEY-VCH Verlag GmbH & Co. KGaA, Weinheim

1 Introduction Thermoelectric (TE) materials have attracted renewed attention in recent years owing to their potential applications in solid-state electronic cooling and power generation with many advantages, such as environmental friendliness, high reliability, and silent operation without moving parts. The efficiency of a TE material in aforementioned applications is determined by the dimensionless figure of merit, defined as $ZT = (S^2\sigma/\kappa)T$, where S, σ, κ, and T are Seebeck coefficient, electrical conductivity, thermal conductivity, and absolute temperature, respectively [1–3]. Therefore, an ideal TE material with high ZT value requires a large Seebeck coefficient, high electrical conductivity, and low thermal conductivity. To improve the TE properties of TE materials, two current methods employed are nanotechnology and energy band engineering [4, 5]

Bismuth telluride (Bi_2Te_3) based alloys are one of the best TE materials used at room temperature. In particular, semiconducting behavior of bismuth telluride alloys can be adjusted by elements doping [5]. For example, Sb doping results in a p-type semiconductor, while Se doping results in an n-type semiconductor. This is ideal for practical applications since both types are needed to make coupled pairs in TE devices. Recently a lot of experiments have been done to enhance TE properties of Bi_2Te_3-based alloys. For example, Cao et al. [6] utilized hydrothermal method and hot-pressing to prepare nanostructured $(Bi,Sb)_2Te_3$ bulk samples which show a high ZT value of 1.28 at 303 K. Wang et al. [7] also successfully employed the melt spinning combined with subsequent spark plasma sintering technique to fabricate nanostructured n-type $Bi_2(Te,Se)_3$ samples which show a maximum ZT of 1.05 at about 420 K. Poudel et al. [8] showed that a peak ZT of 1.4 at 373 K could be achieved in a p-type nanocrystalline BiSbTe bulk alloy made by the ball-milling followed by hot-pressing.

Nanostructure is an effective way to improve TE performance as a consequence of the high TE power and suppressed thermal conductivity in the low-dimensional nanostructures [9]. Due to the advantages of low cost, less device-dependence and large-scale synthesis, hydrothermal method [6, 10, 11] has been widely used to prepare nanostructured bismuth telluride-based alloys. Doping bismuth telluride-based alloys with rare earth metals is another possible way to improve the TE properties [1, 11, 12]. To the best of our knowledge, the reports of nanostructured bismuth telluride-based alloys with different morphologies doped by cerium are rare. So in the present work, we synthesized $Ce_xBi_{2-x}Te_{2.7}Se_{0.3}$ by hydrothermal method. Then the effects of the Ce doping on the morphologies and TE properties were investigated. The results show that Ce doping has significant effects on the morphologies and TE properties. The Ce doping can change the morphologies of

© 2013 WILEY-VCH Verlag GmbH & Co. KGaA, Weinheim

the nanopowders and increase the electrical conductivity remarkably.

2 Experimental Analytical grade of chemicals $Ce(NO_3)_3 \cdot 6H_2O$, $Bi(NO_3)_3 \cdot 5H_2O$, and 5 N pure Se and Te powder were used as the precursors for the synthesis of cerium-doping $Bi_2Se_{0.3}Te_{2.7}$. The precursors with the nominal compositions of $Ce_xBi_{2-x}Se_{0.3}Te_{2.7}$ ($x = 0$–0.3, respectively) were put into a Teflon-lined autoclave filled with about 400 mL distilled water. As an example, in a typical $Ce_{0.2}Bi_{1.8}Se_{0.3}Te_{2.7}$ experiment running, 400 mL aqueous solution containing 18 mmol $Bi(NO_3)_3 \cdot 5H_2O$, 2 mmol $Ce(NO_3)_3 \cdot 6H_2O$, 27 mmol Te powders and 3 mmol Se powders. And then about 3.5 g $NaBH_4$ was added as the reductant, 8 g NaOH as the pH-value controller and 2 g ethylenediaminetetraacetic disodium salt (EDTA) as the organic complexing reagent. The autoclave was then sealed and maintained at 423 K for 24 h. During the reaction, the solution was stirred by a stainless steel stirrer with a rotational speed of about 360 rpm. After the system was cooled down to room temperature, the obtained dark gray powders were filtered, washed with distilled water, ethanol and acetone for several times to remove the residual precursors and by-products. Then the powders were dried in vacuum at 373 K for 6 h. Finally, the resultant powders were hot-pressed into pellets with a diameter of 15 or 12.5 mm at 673 K for 30 min under a pressure of 60 MPa in vacuum.

The phases of the obtained $Ce_xBi_{2-x}Se_{0.3}Te_{2.7}$ powders were identified by X-ray diffraction (XRD) using an X'Pert Pro diffractometer (PANalytical, The Netherlands). The morphologies and compositions of nanopowders were analyzed by field-emission scanning electron microscopy (FESEM) and energy-dispersive X-ray spectroscopy (EDS) on a JSM-6700F microscope (JEM; JEOL, Tokyo, Japan). The density of the samples was measured using the Archimedes method. The electrical conductivity and the Seebeck coefficient were measured at several temperature points by using an LSR-3/800 Seebeck Coefficient/Electric Resistance Measuring System (LINSEIS, Germany) under He atmosphere. The thermal conductivity was measured by a thermal diffusivity system (FLASHLINETM 3000, ANTER Corporation, USA) using Pyroceram (Provided by ANTER) as the reference sample at several temperature points. To avoid the fluctuation in the thermal conductivity measurement several times measurement were perform.

3 Results and discussion Figure 1 shows the XRD patterns of the synthesized $Ce_xBi_{2-x}Se_{0.3}Te_{2.7}$ nanopowders. It indicates that the samples have a single phase of $R\bar{3}m$ rhombohedral structure as that of binary Bi_2Te_3. There are no visible diffraction peaks of Ce and Se or their compounds in the XRD patterns. A representative EDS spectrum of each specimen is shown in Fig. 2. EDS analyses on each specimen was accomplished by collecting spectra from over 15 different nanocrystals and the average values are shown in Table 1. The EDS results indicate that there are Se and Ce in

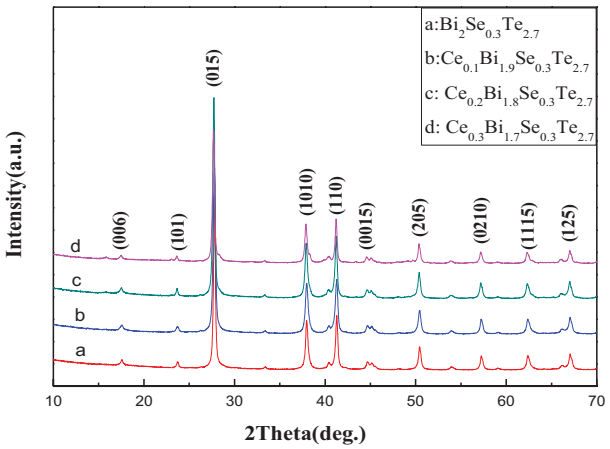

Figure 1 (online color at: www.pss-a.com) XRD patterns of synthesized powders (a) $Bi_2Se_{0.3}Te_{2.7}$; (b) $Ce_{0.1}Bi_{1.9}Se_{0.3}Te_{2.7}$; (c) $Ce_{0.2}Bi_{1.8}Se_{0.3}Te_{2.7}$; (d) $Ce_{0.3}Bi_{1.7}Se_{0.3}Te_{2.7}$.

the samples. With the XRD and EDS results, we concluded that Se and Ce are really incorporated into Bi_2Te_3. Table 1 shows that the actual compositions of all samples are close to the nominal composition. The lattice constants of $Ce_xBi_{2-x}Se_{0.3}Te_{2.7}$ compounds are calculated by Rietveld refinement and are shown in Table 2. Compared to the lattice parameters of Bi_2Te_3 given by JCPDS15-0863 card, $a = 4.385$ Å, $c = 30.48$ Å, the lattice constants of the $Ce_xBi_{2-x}Se_{0.3}Te_{2.7}$ nanopowders are all shorter than them, which is mainly due to the smaller atomic radius of selenium (1.15 Å) compared with that of tellurium (14 Å). In addition, with increasing Ce content, the lattice parameters all increase. The little change for the alloyed crystal structures can be contributed to the small differences between the atomic radius of cerium (1.85 Å) and bismuth (1.60 Å).

Figure 3 shows the morphologies of the synthesized nanopowders. From Fig. 3(a) and (b) it can be seen that the powders are nanosheet agglomerates and the average size is about 100 nm. As reported in Ref. [11], Bi_2Te_3 has a layered hexagonal structure with Te and Bi atom layers arranged in the order of –Te(1)–Bi–Te(2)–Bi–Te(1)-along the *c*-axis. Between two Te(1)-layers there are van der Waals bonds, while all others are covalent bonds. As the energy to break a covalent bond is much higher than that to break a van der Waals bond, Bi_2Te_3 crystal grows much faster along a-axis and *b*-axis than that along *c*-axis. Thus flake morphology is easy formed in natural growth process. Since in our experiments the EDTA was used as surfactant, as reported in Ref. [13] this surfactant would facilitate the growth of Bi_2Te_3 nanosheets along the surface of its agglomerates and help the structure-directing growth of the Bi_2Te_3 nanosheets. However, with increasing Ce content the morphologies change from nanosheets to nanorods as shown in Fig. 3(c) and (d). It indicates that Ce doping has significant effect on the morphologies of the nanopowders. It is not very clear known at present why Ce doping can change the morphologies significantly. The possible reason may be that the replacing

© 2013 WILEY-VCH Verlag GmbH & Co. KGaA, Weinheim

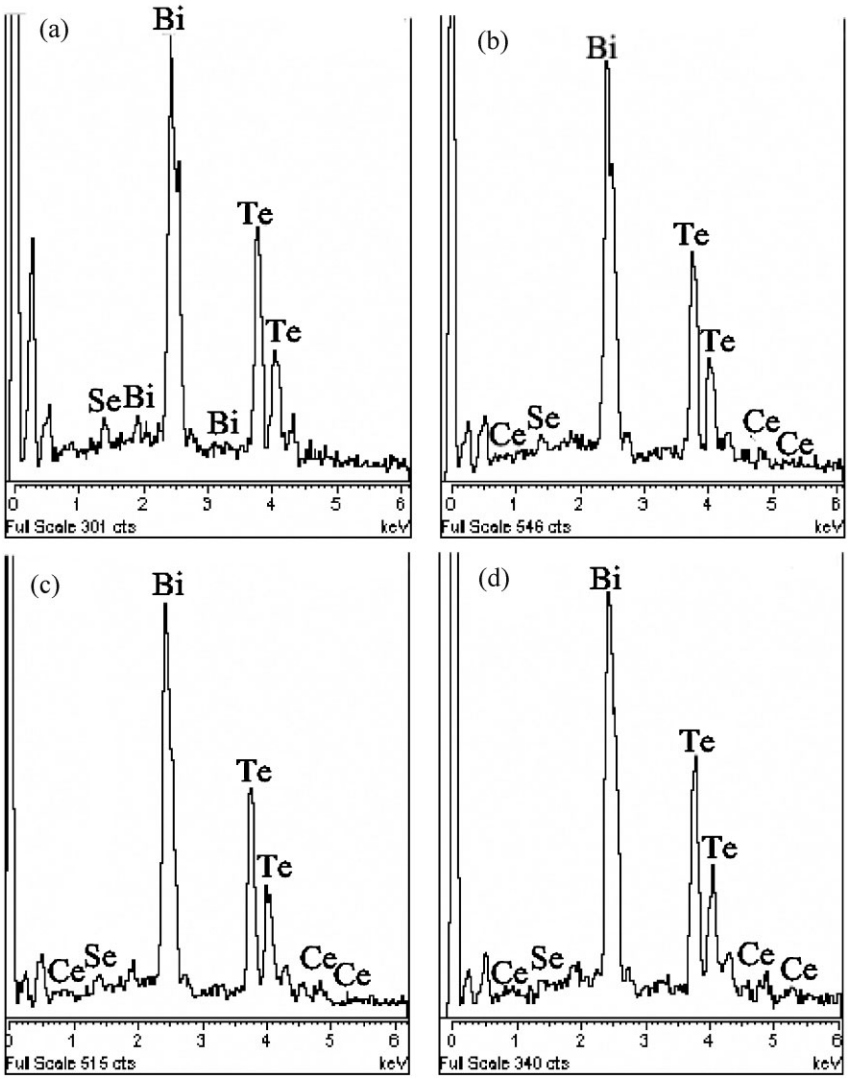

Figure 2 A representative EDSs in the selected regions in synthesized powders (a) $Bi_2Se_{0.3}Te_{2.7}$; (b) $Ce_{0.1}Bi_{1.9}Se_{0.3}Te_{2.7}$; (c) $Ce_{0.2}Bi_{1.8}Se_{0.3}Te_{2.7}$; (d) $Ce_{0.3}Bi_{1.7}Se_{0.3}Te_{2.7}$.

Table 1 The average chemical composition in different areas of the nanopowders measured by EDS.

sample	at%			
	Se	Te	Ce	Bi
$Bi_2Se_{0.3}Te_{2.7}$	5.91(1.23)	54.92(2.16)	0	40.16(2.85)
$Ce_{0.1}Bi_{1.9}Se_{0.3}Te_{2.7}$	5.52(1.26)	54.94(5.09)	2.34(0.47)	40.20(2.26)
$Ce_{0.2}Bi_{1.8}Se_{0.3}Te_{2.7}$	6.37(1.56)	56.91(5.37)	3.88(0.58)	38.25(2.91)
$Ce_{0.3}Bi_{1.7}Se_{0.3}Te_{2.7}$	6.19(1.48)	56.69(4.89)	6.24(1.22)	35.78(4.03)

Table 2 Lattice parameters of synthesized powders.

sample	$Bi_2Se_{0.3}Te_{2.7}$	$Ce_{0.1}Bi_{1.9}Se_{0.3}Te_{2.7}$	$Ce_{0.2}Bi_{1.8}Se_{0.3}Te_{2.7}$	$Ce_{0.3}Bi_{1.7}Se_{0.3}Te_{2.7}$
a (Å)	4.375(±6)	4.377(±8)	4.378(±5)	4.379(±7)
c (Å)	30.43(±3)	30.44(±4)	30.47(±3)	30.48(±2)

© 2013 WILEY-VCH Verlag GmbH & Co. KGaA, Weinheim

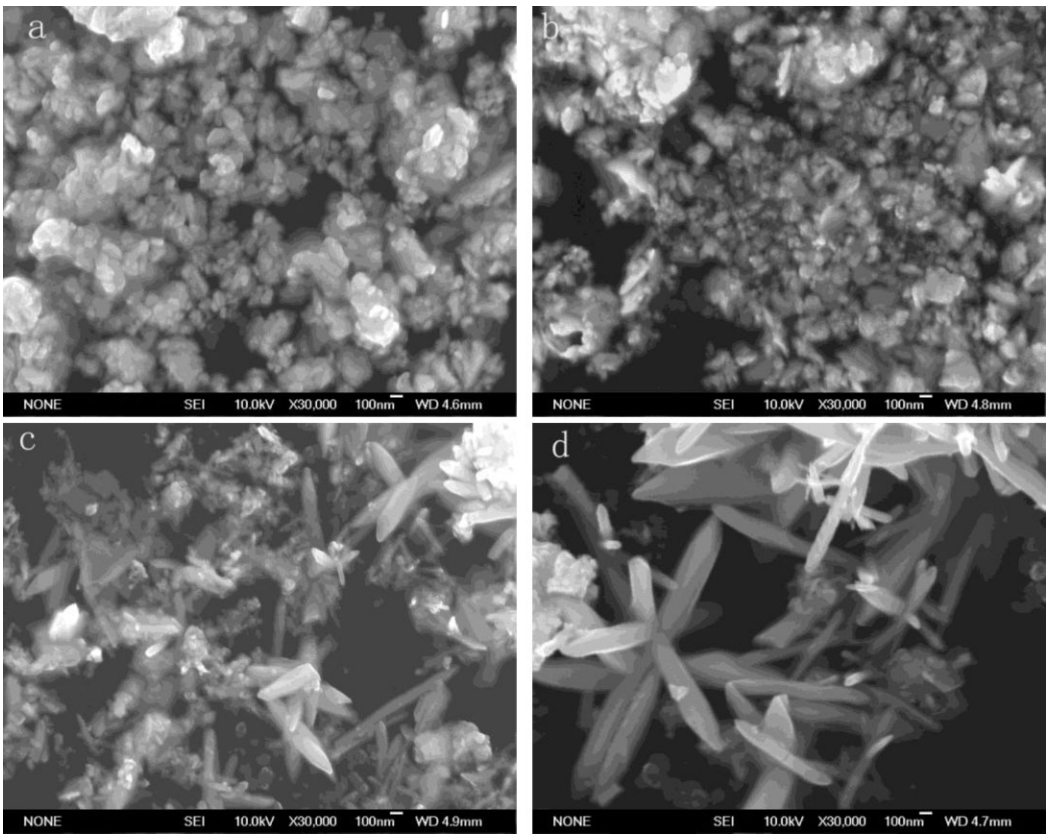

Figure 3 SEM images of synthesized powders (a) $Bi_2Se_{0.3}Te_{2.7}$; (b) $Ce_{0.1}Bi_{1.9}Se_{0.3}Te_{2.7}$; (c) $Ce_{0.2}Bi_{1.8}Se_{0.3}Te_{2.7}$; (d) $Ce_{0.3}Bi_{1.7}Se_{0.3}Te_{2.7}$.

Bi by Ce can change the bonds strength and affect the growth rate along a-axis, b-axis, and c-axis.

Figure 4 shows the microstructures of the hot-pressed bulk samples, which indicates that the samples are compacting. The measured densities are 7.39, 7.35, 7.30, and 7.27 $g\,cm^{-3}$ for samples $x = 0$–0.1, 0.2, and 0.3, respectively. (The calculated theoretical densities of $Bi_2Se_{0.3}Te_{2.7}$ by the Rietveld structural refinement were 7.78 $g\,cm^{-3}$.) In $x = 0$ and 0.1 samples the sheet crystals grow up significantly due to the hot-pressing. In $x = 0.2$ and 0.3 samples the nanorods are disappeared. It can be inferred that nanorods are broken into sheets and then grow up during the hot-pressing. However, the thickness of the sheet crystals is still less than 100 nm, which should be beneficial for the improvement of the TE properties of Bi_2Te_3-based alloys.

Figure 5 shows the electrical conductivities of the samples. It can be seen that Ce doping can increase the electrical conductivity greatly. Especially, an optimum doping value $x = 0.2$ exists, for which the electrical conductivity rising most. It is also worth to note that Ce doping change the variation trend of the electrical conductivity with temperature. The electrical conductivity of the undoped sample increases with increasing temperature, which shows an inherent semiconductor property. While, for the Ce-doped samples their electrical conductivities decrease slightly with increasing temperature, which exhibits a degenerate semiconductor characteristic. This suggests that Ce doping can increase the electron concentrations, although more detailed investigation should be done to determine the nature of Ce in Bi_2Te_3 alloys. The different morphologies of synthesized powders may also be a possible reason to lead to different electrical conductivities [14].

Figure 6 shows the temperature dependences of Seebeck coefficients. All samples with and without Ce doping exhibit as n-type semiconductors since they all have negative Seebeck coefficients in the measured temperature range as shown in Fig. 6. It can be seen that the Ce doping causes a shift of the Seebeck coefficient peak, from 292 to 373, 413, and 433 K as the cerium content increases from $x = 0$ to 0.1, 0.2, and 0.3 respectively. This is a typical behavior in TE materials since the increased external major carriers suppress the generation of minor carriers and hence increase the onset temperature of bipolar effect [4]. Opposite to the electrical conductivity, Ce doping decreases the Seebeck coefficients at lower temperature. This is due to the relationship between Seebeck coefficient and electrical conductivity. For metals or degenerate semiconductors (parabolic band, energy-independent scattering approximation) the Seebeck coefficient is given by [5]

$$S = (8\pi^2 k_B^2/3eh^2)m^* T(\pi/3n)^{2/3}, \quad (1)$$

where n is the carrier concentration and m^* is the effective mass of the carrier. The electrical conductivity (σ) is related

© 2013 WILEY-VCH Verlag GmbH & Co. KGaA, Weinheim

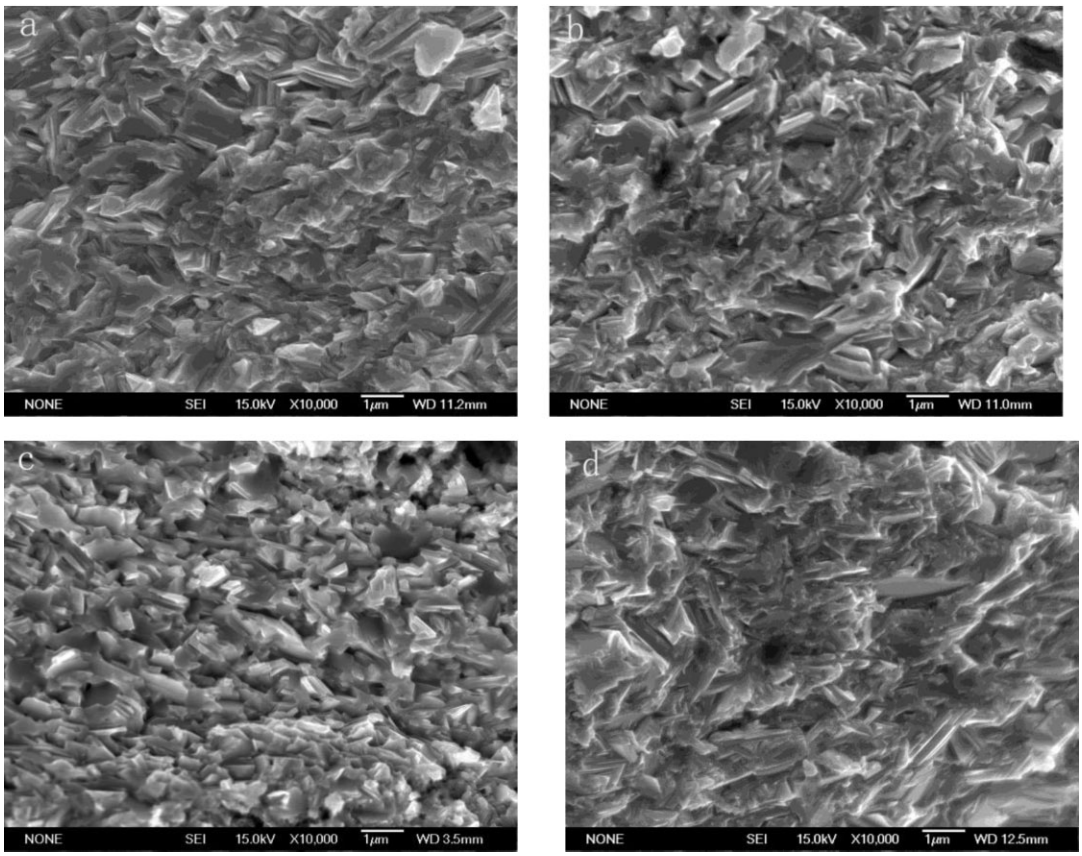

Figure 4 SEM images of the hot-pressed samples; (a) $Bi_2Se_{0.3}Te_{2.7}$; (b) $Ce_{0.1}Bi_{1.9}Se_{0.3}Te_{2.7}$; (c) $Ce_{0.2}Bi_{1.8}Se_{0.3}Te_{2.7}$; (d) $Ce_{0.3}Bi_{1.7}Se_{0.3}Te_{2.7}$.

to n through the carrier mobility μ:

$$\sigma = \mu n e. \tag{2}$$

From the dependence of S, σ on n, normally, low carrier concentration will result in a high Seebeck coefficient. This is the reason for the reduction of the Seebeck coefficients of the Ce doped samples at lower temperature. However, as shown in Fig. 6 the Seebeck coefficients of the doped samples are higher than the undoped one at higher temperature. The reason may be that the Ce substituting for Bi in the alloys introduces a number of defects, which can

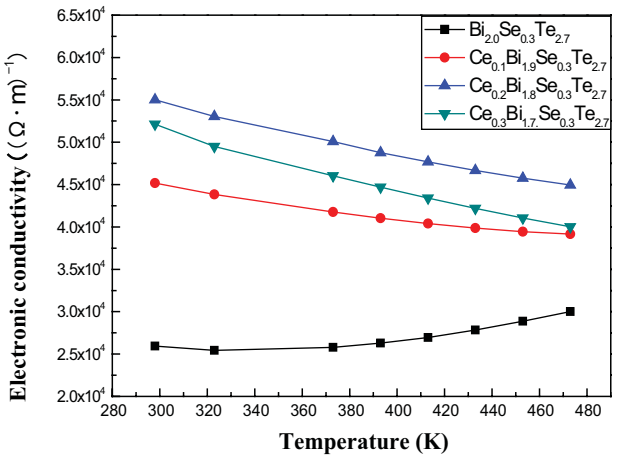

Figure 5 (online color at: www.pss-a.com) Electrical conductivity of hot-pressed $Ce_xBi_{2-x}Se_{0.3}Te_{2.7}$.

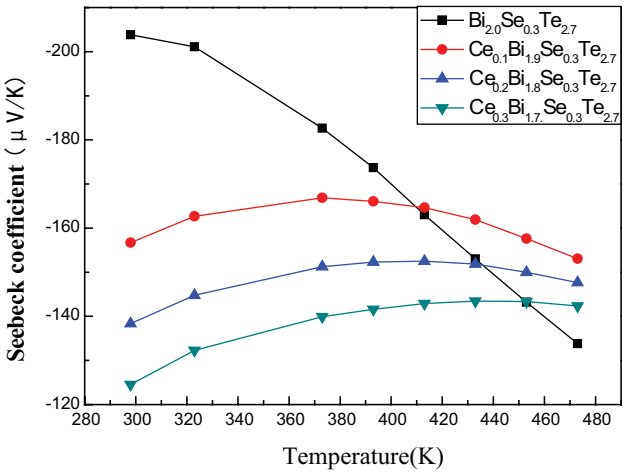

Figure 6 (online color at: www.pss-a.com) Seebeck coefficient of hot-pressed $Ce_xBi_{2-x}Te_{2.7}Se_{0.3}$.

© 2013 WILEY-VCH Verlag GmbH & Co. KGaA, Weinheim

intensify the alloy scattering for the carrier and lead to a larger scattering parameter γ, which can increase the Seebeck coefficient [15]. With increasing temperature the scattering due to Ce doping may be more effective, so the Seebeck coefficients of the doped samples will exceed the undoped sample at elevated temperature.

Observing the results of the electrical conductivity and Seebeck coefficient of the doped samples, it can be found that the electrical conductivity for the $x = 0.2$ sample is larger than that the $x = 0.3$ sample; While the Seebeck coefficient of the $x = 0.2$ sample is higher than the $x = 0.3$ sample. This seems in conflict with the conclusion that a higher electrical conductivity will result in a lower Seebeck coefficient. The possible reason may be as follows: From Eq. (2) the electrical conductivity is co-affect by both n and μ. Lower carrier mobility will also result in lower electrical conductivity and not affect the Seebeck coefficient. Therefore, the lower electrical conductivity but not having a corresponding higher Seebeck coefficient for the $x = 0.3$ sample may be caused by its lower carrier mobility. There are two possible reasons for the lower carrier mobility of the $x = 0.3$ sample: firstly, the Ce doping can enhance carrier scattering, which will reduce the carrier mobility. Secondly, the properties of chemical bonds should significantly influence the carrier mobility. Generally, covalent bond is more favorable for the transport of carriers compared with ionic component [5]. Based on the traditional Pauling empirical formula and the electronegativities of both bonding atoms, the proportion of ionic component of the A–B bond can be estimated by the following equation:$1 - \exp[-(x_A - x_B)^2/4]$, where x_A and x_B are electronegativities of A and B atoms, respectively [16]. According to the electronegativities for the three atoms: cerium (1.12), bismuth (2.02), and tellurium (2.10), it can be calculated that CeTe (21.3%) bond displays much more ionic component than BiTe bond (0.16%), so $Ce_{0.3}Bi_{1.8}Se_{0.3}Te_{2.7}$ possessing more ionic component shows much lower carrier mobility than $Ce_{0.2}Bi_{1.8}Se_{0.3}Te_{2.7}$. Therefore, the electric conductivity of the $x = 0.3$ sample is lower than that of the $x = 0.2$ sample.

Figure 7 shows the thermal conductivities of the samples with temperature. It indicates that the values of the samples are all lower than that of bulk Bi_2Te_3 made by the traditional zone-melted method, which is consistent with many reports on nanostructured Bi_2Te_3 [6–8, 17]. There are two possible reasons for it: (1) the grain size in $Ce_xBi_{2-x}Te_{2.7}Se_{0.3}$ samples is much smaller than that in bulk Bi_2Te_3 as shown in Fig. 4. Theories and experiments indicate that the thermal conductivity decreases with grain size in the TE bulk materials due to numerous boundaries or interfaces are introduced in bulk nanograined materials such that phonons are highly scattered [18]. (2) The doping of Ce will cause a mixed occupancy of the cation positions which also leads to effective phonon scattering due to mass and strain fluctuations. It also indicates that Ce doping will also affect the thermal conductivity correspondingly. At lower temperature of the measured range, it seems that the Ce doping has no help to lower the thermal conductivity. While at high

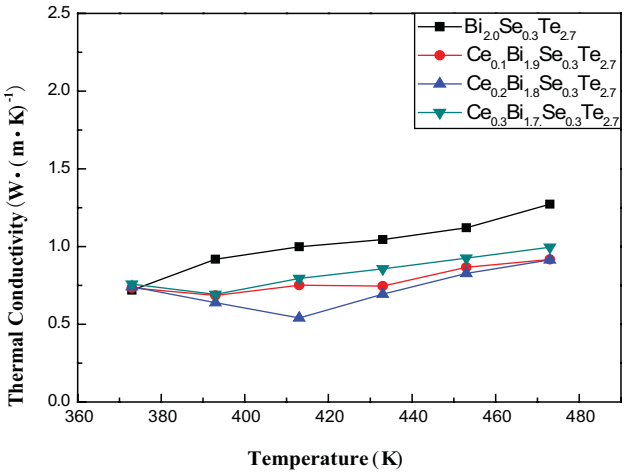

Figure 7 (online color at: www.pss-a.com) Thermal conductivity of hot-pressed $Ce_xBi_{2-x}Te_{2.7}Se_{0.3}$.

temperature the thermal conductivities of the doped samples are a little lower than the undoped sample. This may indicate that phonon scattering due to Ce doping is more effective at high temperature, which is consistent with the results of Seebeck coefficients.

The dimensionless figure of merit ZT was calculated by using the measured values of S, σ, and κ as shown in Fig. 8. Due to the detrimental bipolar effects, the ZT values of the Ce doped samples firstly increase and then decrease with increasing temperature. They all reach the peak value at 413 K. The optimum doped $x = 0.2$ sample shows the highest ZT value of 0.85 at 413 K, which is higher than the Bi_2Te_3 ingot made by the traditional zone-melted method (as shown in Ref. [7]) and is also higher than some rare-earth doped samples [10, 12]. Although it is not as high as samples made by some special technologies [15, 19], maybe the Cerium doping can further enhance the TE properties of the Bi_2Te_3-based alloys if combining with these special technologies.

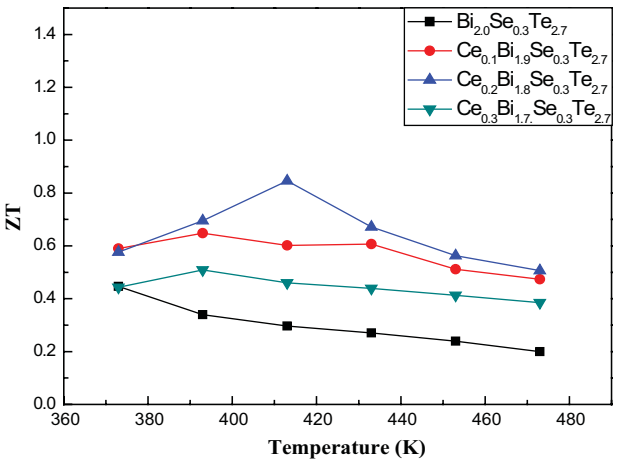

Figure 8 (online color at: www.pss-a.com) ZT values of hot-pressed $Ce_xBi_{2-x}Se_{0.3}Te_{2.7}$.

© 2013 WILEY-VCH Verlag GmbH & Co. KGaA, Weinheim

4 Conclusions $Ce_xBi_{2-x}Se_{0.3}Te_{2.7}$ ($x = 0$–0.3) nanopowders were synthesized by the hydrothermal method. The doping of Ce will not cause impure phases, but dependent on the Ce content the morphologies of the nanopowders will change remarkably. The TE property measurements of the hot-pressed samples reveal that Ce doping can increase the electrical conductivity remarkably, but has little effect on improving Seebeck coefficient and thermal conductivity. The optimum Ce content should be around $x = 0.2$ which can result in a highest ZT of 0.85 at 413 K.

References

[1] F. J. Disalvo and F. J. Disalvo, Science **285**, 703 (1999).
[2] J. R. Sootsman, D. Y. Chung, and M. G. Kanatzidis, Angew. Chem., Int. Ed. **48**, 8616 (2009).
[3] L. E. Bell, Science **321**, 1457 (2008).
[4] A. J. Minnich, M. S. Dresselhaus, Z. F. Ren, and G. Chen, Energy Environ. Sci. **2**, 466 (2009).
[5] G. J. Snyder and E. S. Toberer, Nature Mater. **7**, 105 (2008).
[6] Y. Q. Cao, T. J. Zhu, X. B. Zhao, X. B. Zhang, and J. P. Tu, Appl. Phys. A **324**, 321 (2008).
[7] S. Y. Wang, W. J. Xie, H. Li, and X. F. Tang, Intermetallics **19**, 1024 (2011).
[8] B. Poudel, Q. Hao, Y. Ma, Y. Lan, A. Minnich, B. Yu, X. Yan, D. Wang, A. Muto, D. Vashaee, X. Chen, J. Liu, M. S. Dresselhaus, G. Chen, and Z. Ren, Science **320**, 634 (2008).
[9] M. Dresselhaus, G. Dresselhaus, X. Sun, Z. Zhang, S. B. Cronin, T. Koga, J. Y. Ying, and G. Chen, Microscale Thermophys. Eng. **3**, 89 (1999).
[10] X. B. Zhao, X. H. Ji, Y. H. Zhang, T. J. Zhu, J. P. Tu, and X. B. Zhang, Appl. Phys. Lett. **86**, 062111 (2005).
[11] Y. H. Zhang, T. J. Zhu, J. P. Tu, and X. B. Zhao, Mater. Chem. Phys. **103**, 484 (2007).
[12] X. H. Ji, X. B. Zhao, Y. H. Zhang, B. H. Lu, and H. L. Ni, J. Alloy. Compd. **387**, 282 (2005).
[13] Y. Deng, C. W. Nan, G. D. Wei, L. Guo, and Y. H. Lin, Chem. Phys. Lett. **374**, 410 (2003).
[14] Q. Zhao and Y. G. Wang, J. Alloy. Compd. **497**, 57 (2010).
[15] W. S. Liu, Q. Y. Zhang, Y. C. Lan, S. Chen, X. Yan, Q. Zhang, H. Wang, D. Z. Wang, G. Chen, and Z. F. Ren, Adv. Energy Mater. **1**, 577 (2011).
[16] M. L. Bhatia, Intermetallics **7**, 641 (1999).
[17] X. H. Ji, X. B. Zhao, Y. H. Zhang, B. H. Lu, and H. L. Ni, Mater. Lett. **59**, 682 (2005).
[18] Y. C. Lan, A. J. Minnich, G. Chen, and Z. F. Ren, Adv. Funct. Mater. **20**, 357 (2010).
[19] X. Yan, B. Poudel, Y. Ma, W. S. Liu, G. Joshi, H. Wang, Y. C. Lan, D. Z. Wang, G. Chen, and Z. F. Ren, Nano Lett. **10**, 3373 (2010).

© 2013 WILEY-VCH Verlag GmbH & Co. KGaA, Weinheim